TIME-RESOLVED X-RAY DIFFRACTION STUDY OF PHOTOSTIMULATED PURPLE MEMBRANE

ROBERT D. FRANKEL AND JAMES M. FORSYTH
Laboratory for Laser Energetics, College of Engineering and Applied Sciences, University of Rochester, Rochester, New York 14623

ABSTRACT A nanosecond resolution laser-driven x-ray source has been used to perform a time-resolved, x-ray diffraction study of the purple membrane of the *Halobacterium halobium*. Alterations in diffraction patterns have been observed 1 ms after photostimulation, and are interpreted to show disorder of bacteriorhodopsin packing in the plane of the membrane with little bacteriorhodopsin structural change.

INTRODUCTION

Investigation of the conformational flexibility and dynamics of proteins and assemblies of proteins is essential to understand biological function. Until recently x-ray diffraction studies of proteins have not examined dynamic structures. Now, using new synchrotron x-ray sources, investigators have begun to probe protein dynamics. Studies of contracting muscle have been particularly successful (1), because contraction can be initiated repetitively, permitting signal averaging to obtain millisecond resolution. Unfortunately, many samples cannot recycle, limiting resolution to typical synchrotron exposure times of 100 ms.

To provide higher time resolution, we have developed a low-angle x-ray diffraction camera that is irradiated by a laser plasma x-ray source (2–5). The laser plasma is an intense, nanosecond duration, roughly isotropic, point source of x rays. The x-ray camera's high numerical aperture and sensitive x-ray detection system permits acquisition of single shot diffraction patterns of high statistical significance, making possible nanosecond to millisecond resolution diffraction studies on samples that cannot recycle.

The purple membrane (PM) of the *Halobacterium halobium* is the first system we have examined with the laser plasma x-ray source. PM has a photocycle of well-defined photochemical intermediates, as well as being a 2-dimensional hexagonal lattice composed of one protein, bacteriorhodopsin (BR) (6). It is well established that BR acts as a light driven, transmembrane hydrogen ion pump (7). Henderson and Unwin (8) have shown that BR is composed of seven α-helices arrayed roughly perpendicular to the membrane plane, with BR's arranged in three-fold symmetric trimers.

We have examined photostimulated PM during the M_{412} photointermediate, 1 ms after stimulation, a time when others have observed experimental signatures related to proton pumping and membrane conformational flexibility (9–11).

Most of our data were obtained from vacuum-dried samples, although low resolution results from hydrated membranes are also presented. Dried PM undergoes a photocycle (12, 13), and has been used in studies involving electrical potential generation (14), infrared Fourier transform (15, 16), and absorption spectroscopies (12). We have observed similarities in stimulated x-ray diffraction patterns between dried and hydrated specimens. Hence, we believe dried membrane results are relevant to analysis of hydrated PM structural kinetics.

In hydrated PM kept in the dark, 50% of the BR attached retinal converts from the all-*trans* light-adapted structure to the 13-*cis* dark adapted form. At low humidity the light driven back reaction of 13-*cis* to all-*trans* retinal is blocked (13). Thus most samples were light adapted until 1–3 min before stimulation and acquisition of x-ray diffraction patterns.

Our results show major alterations in x-ray scattering patterns from light-adapted specimens after stimulation. Based upon modeling and radial autocorrelation analysis, we argue the changes observed reflect disorder of monomers or trimers upon stimulation with little if any monomer structural change to 7-Å resolution.

TECHNIQUES

The laser plasma x-ray source and attached toroidal x-ray camera system, under development at the Laboratory for Laser Energetics (LLE) for several years, will be described in full elsewhere. Here we briefly review major aspects of the system.

The intense optical field of a focused laser accelerates electrons in solids producing an electron avalanche and turning the solid into a hot plasma. At focused powers of 10^{14} W/cm^2 or higher, laser light absorption in the plasma produces electron temperatures greater than 1 keV, yielding highly stripped plasma ions. Significant collisional production of x-ray radiation occurs, including high-brightness line radiation from the plasma ions. The radiation is emitted on the same time scale as the laser heating pulse (for pulses longer than 10^{-10} s) from the region the size of the focal volume of the target illumination system.

A single beam, multistage, neodynium glass laser, named the Glass Development Laser (GDL) (17), was used to create the x-ray source. GDL produced pulses of 1.054 μm radiation of ~1.1 ns FWHM at energies up to 120 joules. Soft x-ray (i.e., $h\nu \gtrsim 5$ kev) production from a plasma is enhanced when the heating laser's wavelength is shortened (18). An efficient system of third harmonic generation from high power laser pulses has been developed at LLE (19) and implemented on GDL. This system permits delivery of up to 60 joules of energy at 0.351 μm to targets in a 100 μm diam spot at intensities up to 10^{15} W/cm^2. This plasma is produced in a chamber held at a pressure of 10^{-5} torr. Single x-ray line emission may exceed 1% of the incident laser energy.

The x-ray line emission is monochromatized at discrete wavelengths by foil filtration in the camera. Our experiments employed Cl^{+15} line radiation at 4.45 Å ($\Delta\lambda/\lambda$ of 8×10^{-3}) using saran ($C_2H_2Cl_2$) targets for plasma production and saran foil filtration. At 4.45 Å the x-ray absorption length in PM (50 μm) is closely matched to the optical extinction distance near 530 nm, facilitating preparation of highly photostimulated structures exhibiting optimum x-ray scattering efficiency.

Since the soft x-ray emission from the plasma is confined to the laser focal volume, we may use efficient, toroidal x-ray optics to collect and focus the x-ray radiation (20, 21). We fabricated a toroid 9 cm long and 2 cm i.d. having a focal length of 86 cm, polished in a CERVIT® substrate, and coated with nickel. This mirror efficiently reflected x-rays up to ~6 keV while keeping a convenient, annular beam diameter at typical sample positions. Approximately 10^{10} photons at 4.45 Å were delivered to a specimen on one shot.

X-rays were recorded using a digital, slow scan, intensified television system (22), shown in Fig. 1. X-rays were incident upon an 80 μm thick ZnS(Ag) phosphor deposited (Thomas Electronics, Wayne, NJ) on a tapered fiberoptic faceplate (American Optical Scientific Instruments, Buffalo, NY). One side of the faceplate was ground in the University of Rochester Optical Shop to approximate the focal surface of the x-ray camera. The faceplate was direct coupled to the 50 mm fiberoptic input of a channelplate intensifier (6301; Varo, Inc., Garland, TX) adjusted to a luminosity gain of 40,000. A f/1.9 oscillograph lens (Wollensak Optical, Rochester, NY) imaged the intensifier output image onto the 16 mm input of a 1254 silicon intensified target (SIT) detector (EG & G Princeton Applied Research [PAR], Princeton, NJ). The input to the lens was shuttered by a #4 42.5 mm shutter (Ilex Optical Co., Inc., E. Rochester, NY). During a shot sequence the shutter was gated open for 50 ms by an Ilex speed computer, responding to a command from the GDL control computer. The SIT was kept at −25°C in a PAR 1213 refrigerator to reduce target dark current. Scan instructions were issued to the SIT by a PAR 1216 controller. The 1216 also acquired and digitized the output of each channel of the SIT via a 14 bit A/D. The readout format included 224 lines of 448 channels each. Channel dwell-time was 140 μs; thus a scan required 14 s. Readout consisted of three target scans. The readout electron beam voltage was set to 7.5 V compared to 5.0 V during target preparation. High voltage, multiple scan readout provided more complete image readout with increased dynamic range (23, 24).

The 1216 controller was interfaced to an LSI 11/23 (Digital Equipment Corporation [DEC], Marlboro, MA) via a DRV-11 parallel interface card. The 11/23 sent scan parameters to the 1216, and summed digitized images into its memory. Images were temporarily stored on a DEC RL-01 hard disk before archival storage on magnetic tape. Data analysis was performed on the 11/23 augmented with a SKYMNK-02 (SKY Computer) array processor. Programming was performed in the computer language FORTH. Data analysis included geometrical correction, intensity correction, circular averaging of circularly symmetric diffraction patterns, and radial autocorrelation analysis.

PM was provided by Dr. Janos Lanyi in either 4 M NaCl or 20% sucrose solution. Samples were washed free of salt or sugar by multiple centrifugations in a Beckman L-5 ultracentrifuge (Beckman Instruments, Inc., Fullerton, CA). The final pellet was suspended in a small volume of H_2O and stored at 4°C. Samples were air dried to 30–60 μm thickness on 1–2 μm polypropylene films prior to experiments. To hydrate specimens, they were placed in a chamber through which we flowed helium raised to 100% humidity by bubbling through water. (Samples were equilibrated in the chamber for 24 h.) The chamber was aligned to the x-ray camera axis by means of He-Ne laser alignment beam having identical geometry to the converging x-ray beam. The plane of the PM was normal to the camera axis.

A 25 μm Saran input window in the specimen chamber acted as an x-ray monochromator, a vacuum window, and a transparent stimulus input window. A 25 μm Beryllium output window served as the other vacuum interface.

We produced the stimulus from a repetitively Q-switched, CW pumped, Nd^{+3}/YAG laser, (model 510; Control Laser Corp., Orlando, FL) amplified by a pulse pumped Nd^{+3}/glass amplifier. The Q-switch was driven by a radio frequency burst generator. Both the burst generator and the amplifier were triggered by signals from the master GDL computer. Synchronized operation of the GDL and stimulus lasers allowed PM stimulation from a few microseconds to 68 ms before the x-ray burst. The amplified pulse train was focused into a temperature-tuned nonlinear crystal to produce second harmonic radiation at 0.532

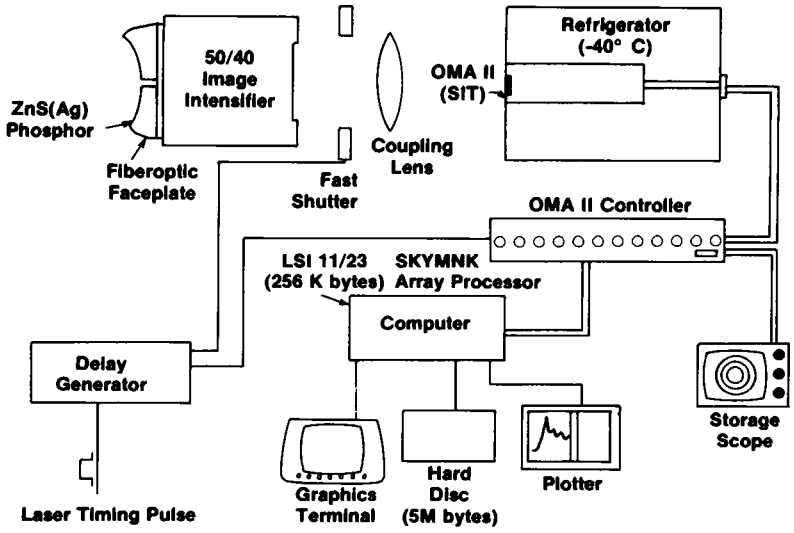

FIGURE 1 X-ray detection system.

μm. The 1.064-μm light was removed from the output by reflection off of four dichroic (multilayer dielectric) mirrors. The green pulses were converted to circular polarization by a quarter wave plate.

The stimulus pulses were delivered to the specimen approximately collinear to the x-ray pulses by an x-ray transmitting mirror consisting of 2,000 Å of aluminum deposited on 1.5 μm thick Mylar. The stimulus laser irradiated a 1 mm^2 area on the specimen.

There exists a light-driven equilibrium between the light-adapted ground state, BR_{568}, and BR's first stable photointermediate, K_{610}, such that only 30% of the molecules absorbing light will photocycle (25, 26). Hence, to maximally populate the M_{412} state, we adopted a multiple pulse stimulated strategy. A train of six, 530 nm, 150 ns FWHM laser pulses with a total train energy of 100–200 μJ was used. The interpulse spacing was 45 μs. The first pulse drove some of the system into the M_{412} state, which has a half time of formation of 40 μs at room temperature. Subsequent pulses photoactivated more BR_{568} molecules while minimally stimulating M_{412} molecules. Investigation of uniphase samples of K_{610} and L_{550} was not possible with this excitation strategy.

RESULTS

During early system tests, many patterns were obtained at low (14 Å) resolution. These were obtained from both hydrated and dried specimens, as well as from stimulated and unstimulated preparations.

Recently, we have obtained higher quality patterns with 7-Å resolution. Both stimulated and unstimulated patterns have been obtained from dried specimens. Improved system performance was primarily due to the use of the curved, tapered fiberoptic faceplate to support the x-ray scintillator.

These experiments used 248 GDL shots. (Laser shots are available to the LLE experimental stations on an assigned schedule at up to two per hour.) Ninety-three shots were consumed on diffraction equipment testing and development. Altogether, 109 shots produced low-resolution diffraction patterns from dried, hydrated, stimulated, and unstimulated specimens. Forty-six shots were taken at high resolution.

Although the x-ray dose of 10^{10} photons per diffraction pattern was modest, we were concerned that the high x-ray dose rates used might damage the PM. We did not observe significant x-ray diffraction pattern degradation after three to four consecutive exposures on dried or hydrated PM stacks. However, to minimize possible x-ray induced results, stimulation experiments were performed on previously unirradiated PM samples.

Fig. 2 displays a circular average of a typical, reproducible, diffraction pattern from unstimulated PM. This pattern was partially corrected for system geometrical distortions as well as for nonuniform sensitivity of the detection system. Compared with published diffraction patterns (27, 28) we have achieved about a factor of 2–3 lower instrumental resolution and somewhat reduced signal-to-noise ratio. However, all of the main orders of diffraction are present at the appropriate intensity ratios and positions.

Disorder

Fig. 3 displays a background-corrected diffraction pattern obtained 1 ms after stimulation of a light-adapted, dried,

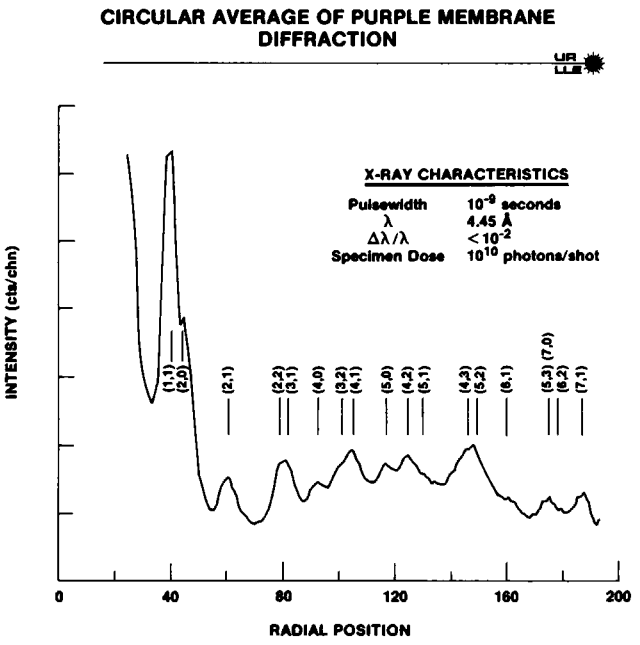

FIGURE 2 Circular average of a dried PM powder pattern. Background scattering was not removed. This sample displayed background scattering caused by cracking on drying. The abscissa is in units of TV channels from the x-ray camera focus. There is some residual detector nonlinearity in the abscissa.

membrane stack. The broad rising and falling background in the 0.05–0.11 $Å^{-1}$ region of the diffraction pattern is indicative of scattering from BR monomers or trimers (29), and is suggestive of significant disorder in the specimen after stimulation. Disorder in the membrane prevents sampling of PM diffraction only at lattice reflections, and allows collection of full monomer or trimer scattering curves. The scattering distribution from monomers initially falls from the zero order and then rises into a broad peak with a maximum at 0.10 $Å^{-1}$, similar to the rising and falling background in Fig. 3. Trimer scattering produces

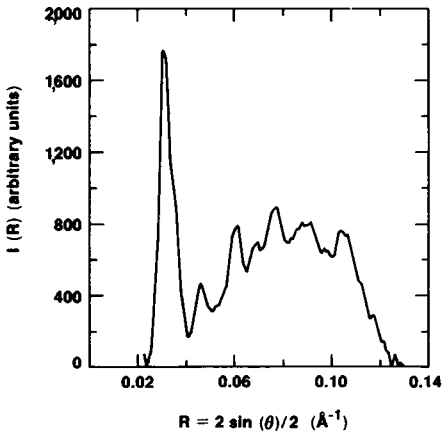

FIGURE 3 Circular average of dried PM x-ray diffraction pattern, one millisecond after stimulation. This pattern was fully corrected for geometric distortion; the monotonically decreasing background was fitted to a cubic function and subtracted from the raw data.

the same broad curve but is modulated by a sinusoid with a period of 0.025 $Å^{-1}$. In addition, a sharper peak is present at 0.03 $Å^{-1}$, related to monomer-monomer interference effects. This feature peaks at a slightly lower angle than the (1, 1) reflection from native PM; however, it is broader than a lattice reflection and hence overlaps the (1, 1) and (2, 0) orders on its high angle side and almost extends to the (1, 0) reflection on the low angle side.

Fig. 4 displays kinetic results obtained at low resolution from both dried and hydrated samples. Note the double peak structure in the 0.03 $Å^{-1}$ region, or (1, 1) region of the pattern. It is unlikely that peak twinning represents the formation of two lattices, because we do not observe a doubling of all orders. More likely, the low angle peak reflects the development of trimer scattering, manifesting a strong peak at 0.03 $Å^{-1}$. In the hydrated case, the low angle peak appeared 1 ms after stimulation, and disappeared in the shot taken 30 min later on the same specimen. In the dried case, we have observed the double peak structure after a strong, single train stimulation, and also after a series of weaker trains, which were delivered minutes apart. In a vacuum, this structure was stable for several hours. After overnight rehydration the original lattice reformed.

For several reasons we believe the disorder observed is not lattice disorder caused by heating due to photostimulation. Calculations indicate that the stimulus-induced temperature rise in the sample should be <5°C. Moreover, the pulse train stimulus scenario limits impulse heating. We suggest that substitution (or unit cell) disorder is the predominant alteration causing the disordered scattering evident in Fig. 3. Trimeric structures may be partially disordered and still yield a 0.03 $Å^{-1}$ peak, or the trimers may move as a unit upon BR activation. We have not observed a pure trimer or pure monomer pattern with the absence of lattice structure.

Coherent diffraction peaks display alteration within 1 ms of stimulation, and in dried samples continue to evolve, such that ½ h after stimulation, patterns are different from the 1 ms patterns. Alterations in the relative intensities of peaks are present throughout the pattern. Significant activity occurs in the 0.07–0.1 $Å^{-1}$ region of scattering.

Fig. 5 displays the 0.05–0.14 $Å^{-1}$ region of four circularly averaged diffraction patterns. Trace 5 *a* is an unstimulated control; 5 *b* is a pattern 1 ms poststimulus, 5 *c* is a pattern 30 min poststimulus, whereas 5 *d* is a pattern obtained after exposure to multiple trains of stimuli. The ratio of peaks in the 0.07–0.1 $Å^{-1}$ region is different in each of the traces shown. Also the ratio of incoherent to lattice-derived scattering rises after stimulation, especially after multiple stimuli.

In powder crystallography studies, structure factor determination requires phase assignment as well as intensity splitting in overlapping orders. Others have used the EM-deduced structure factors (8) to phase and separate intensities in overlapping orders in neutron (30) and x-ray diffraction powder patterns (31) from PM. In altered (kinetic) x-ray diffraction patterns, this approach is not justifiable, because of major alterations in background scattering and the observed peak intensity ratios. However, structural information can be obtained directly from kinetic patterns by computation of the radial autocorrelation function (29). This is the Fourier-Bessel transform of an intensity function with circular symmetry, and is the radial projection of the two-dimensional autocorrelation function. This analysis is particularly relevant to PM, where peaks in the radial autocorrelation function are representative of structures in the static two-dimensional map. In kinetic experiments, change in autocorrelation peaks yields information on real space alterations in these electron density features.

Fig. 6 *a*, *b* displays the radial autocorrelation function of native PM (Fig. 6 *a*) and stimulated PM (Fig. 6 *b*). In both plots, the peaks at 10 Å correspond to the helix-helix

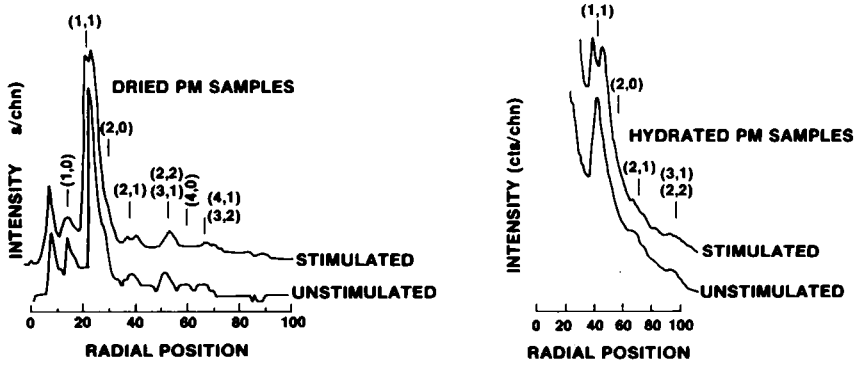

FIGURE 4 Low resolution x-ray diffraction patterns from unstimulated PM. (*A*) Dried specimen: PM was stimulated by a series of three pulse trains spaced 30 min apart. Peak doubling is evident in the (1, 1) region of scattering. The pattern reverted to its unstimulated form after overnight rehydration at atmosphere. (*B*) Hydrated specimen: The unstimulated pattern was obtained 30 min after stimulation. X-ray patterns in prestimulus (not shown) and poststimulus exposes were similar. The low angle peak in the twin reflection appears at a slightly lower angle than the (1, 1) peak in the pattern from the unstimulated PM. The background has not been removed. The high level of background scatter from hydrated specimens was due to membrane stacking disorder at 100% humidity.

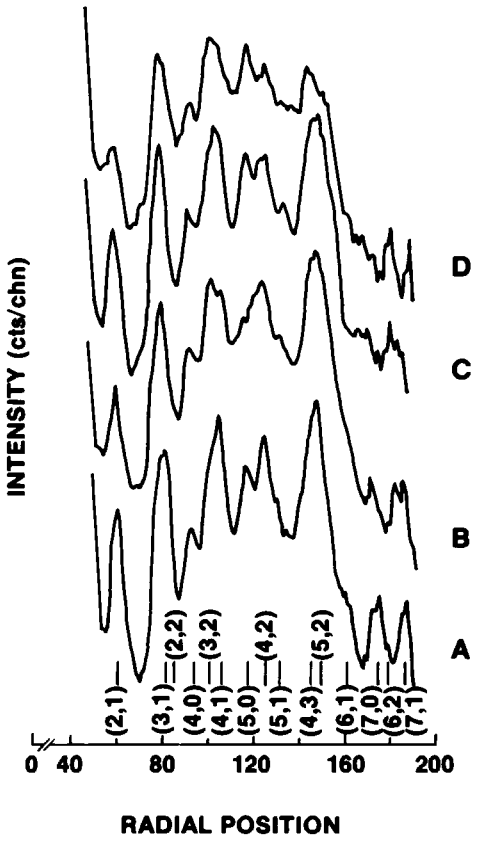

FIGURE 5 Plots of four PM diffraction patterns in the 0.05–0.14 $Å^{-1}$ region. No background subtraction was performed. Some residual detector nonlinearity is present along the x-axis. (A) Unstimulated PM. Some disorder is present due to cracking on drying. (B) 1-ms poststimulation pattern. Note increased background, and alteration in peaks in the (4, 2) (5, 1) and (4, 3) region. Variability in this region was common in patterns from stimulated PM. Scattering at higher angles than the (5, 3) reflection was much reduced. (C) 30-min poststimulation pattern. Further changes in the (4, 2)–(4, 3) region are apparent. (D) Pattern obtained after three-, six-pulse stimulation trains. More change in the (4, 2)–(4, 3) region. There is much more incoherent background.

separation in the BR molecule, the clearest intramolecular signal in the radial autocorrelation function. Comparison of the 10-Å peaks in both functions show little if any difference between stimulated and unstimulated patterns. This comparison reveals that, with regard to helix-helix spacing, no significant intramolecular alterations occur. It is possible however, that small structural alterations are present in the BR helices.

Peaks in the 20–40 Å region of the autocorrelation plots relate to monomer-monomer correlations. Intratrimer monomer-monomer correlation signatures are weak relative to intertrimer correlations, because of poor intratrimer electron density contrast. Monomers in neighboring trimers are separated by a low electron density lipid boundary layer, which provides higher electron density contrast. Thus, peaks represent correlation distances of monomers in different trimers. Alterations are evident in the 20–40 Å region of stimulated PM. These peaks may include contributions from several PM lattice forms (stimulated and unstimulated areas), as well as from disordered areas of PM. Hence, interpretation is extremely difficult. However, we suggest disorder may cause the alterations in monomer-monomer correlation peaks observed in stimulated PM.

DISCUSSION

The most widely accepted framework for proton pumping in PM is the proton wire proposed by Nagle and Morowitz (32). Here protons jump along the α-helical segments of BR until surface exposure. Charge transport may be initiated by the light-induced, *trans-cis* isomerization of BR's retinal, followed by deprotonation of the Schiff-base linkage of retinal to the apoprotein (33). Only small intramolecular conformational change would be needed to provide structural correlates of a switched proton wire. Indeed, in experiments reported here and elsewhere using a variety of techniques, little intramolecular structural alteration has been observed after photostimulation (15, 16, 34–37).

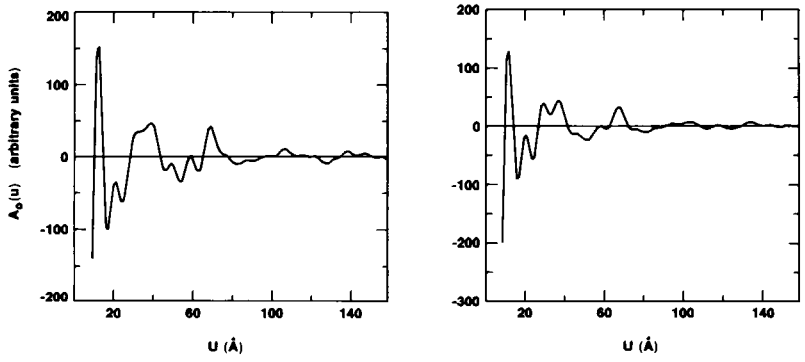

FIGURE 6 Radial autocorrelation functions. For the autocorrelation plots data were taken from PM diffraction patterns that had instrument background subtracted. Nonmonotonically falling background was not removed. Inclusion of the latter background weakens the lattice correlation peaks at greater than 60 Å compared to lower angle peaks. (A) Radial autocorrelation function from unstimulated PM, (B) radial autocorrelation function from diffraction pattern recorded 1 ms after BR stimulation.

On the other hand, some evidence has accumulated with regard to possible BR-BR coupling and longer scale length structural alterations. Transient dichroism studies (11), have shown several different small rotations of BR monomers (<20°) after light absorption. Tokutomi et al. (10) observed a flash-induced transient PM fluidity change with a 1.0 ms half-formation time. Beece et al. report significant viscosity effects on the kinetics of the M–O and O–BR transitions (38). Hess and Korenstein found two occupancy-dependent decay rates for the M_{412} photointermediate (12). Circular dichroism measurements indicate excitonic coupling of chromophores (34). The finding of disorder in our experiments is consistent with the results of Ahl and Cone (1982), and of Tokutomi et al. (1981), and may be related to the work of Korenstein and Hess (1977*a*, *b*).

Alteration in surface potential may provide the motive force for these changes. Along with others, we observe structural changes at the time reported for surface potential alteration (9), i.e., after M_{412} formation. In these experiments (as in those of others) stimulus levels exceeded the natural solar exposure of PM in sea water. In addition, we have worked at low ionic strength. These conditions may maximize surface potential alteration and structural change (9). Future experiments at higher ionic strength in hydrated samples, and at earlier times in the photocycle (before surface potential alteration) will help clarify whether or not surface potential is the motive force for the changes observed.

The potential of the laser plasma as an x-ray source for pulsed diffraction work has just begun to be exploited. These experiments have taken advantage of the ability of the laser plasma to generate copious 4.45 Å radiation, facilitating diffraction from thin samples that can be efficiently photostimulated. Other time-resolved studies, such as contracting muscle, or solution scattering from proteins, may require thicker samples, dictating use of more energetic x rays. Helium-like Ti (at 2.6 Å), Fe (at 1.85 Å) or Ni (at 1.6 Å) are possible choices for emitting ions.

Titanium radiation is produced with one-third the efficiency of He-like Cl radiation (18). The x-ray emission from the harder lines is further reduced. However, GDL will soon be upgraded in energy to 200 J/pulse at 351-nm with the addition of active mirror booster amplifiers (39) and large frequency-tripling crystals. These changes should allow comparable fluxes to be generated at 2.6 Å as are now produced at 4.45 Å.

The laser plasma source should be useful in studies where synchroton time resolution is insufficient. Such studies include shock wave propagation in solids, transient states in chemical reactions, critical phenomena, enzyme-substrate interactions, macromolecular folding as well as events in transmembrane ion pumping. We believe a greatly extended range of investigations of the structural aspects of kinetics is now possible.

We are grateful to Dr. J. Lanyi for the PM preparations, to F. Kirkpatrick, B. Fung, and M. Nicholson for facilities for washing the PM, to J. Abate, B. Flaherty, W. Lockman, and T. Kessler for operating the laser, to L. Forsley for assistance in computer programming, and to J. K. Blasie for suggesting that we examine reference 29.

This work was supported, in part, by the National Science Foundation, grant PCM 79-04375, and by the National Institutes of Health, grant 1R01 GM-27354-01. This work was partially supported by the following sponsors: Empire State Electric Energy Research Corporation, Exxon Research and Engineering Company, General Electric Company, New York State Energy Research and Development Authority, Northeast Utilities, The Standard Oil Company (OHIO), and The University of Rochester. Such support does not imply endorsement of the content by any of the above parties.

Received for publication 12 March 1984 and in final form 25 September 1984.

REFERENCES

1. Huxley, H. E., A. R. Faruqi, J. Bordas, M. H. J. Koch, and J. R. Milch. 1980. The use of synchroton radiation in time resolved x-ray diffraction studies of myosin layer line reflections during muscle contraction. *Nature (Lond.)*. 284:140–143.
2. Frankel, R. D., and J. Forsyth. 1979. Nanosecond x-ray diffraction from biological samples with a laser-produced plasma source. *Science (Wash. DC)*. 204:622–624.
3. Forsyth, J., and R. D. Frankel. 1982. Nanosecond exposure x-ray diffraction patterns from biological specimens using a laser plasma source. *Biophysics*. 37:73*a*.
4. Frankel, R. D., and J. M. Forsyth. 1982. Application of nanosecond x-ray diffraction techniques to bacteriorhodopsin. *Methods Enzymol.* 88:276–281.
5. Frankel, R. D., and J. M. Forsyth. 1982. Time resolved x-ray diffraction studies on purple membrane from *Halobacterium halobium*. *Biophys. J.* 37(2, Pt. 2):232*a*. (Abstr.)
6. Blaurock, A. E., and W. Stoeckenius. 1971. Structure of the purple membrane. *Nat. New Biol.* 233:152–155.
7. Lozier, H., R. A. Bogomolni, and W. Stoeckenius. 1975. Bacteriorhodopsin. A light-driven proton pump in *Halobacterium halobium*. *Biophys. J.* 15:955–962.
8. Henderson, R., and P. N. T. Unwin. 1975. Three-dimensional model of purple membrane obtained by electron microscopy. *Nature (Lond.)*. 257:28–32.
9. Cafiso, D. S., W. L. Hubbel, and A. Quintanilha. 1982. Spin-label probes of light-induced electrical potentials in rhodopsin and bacteriorhodopsin. *Methods Enzymol.* 88:682–696.
10. Tokutomi, S., T. Iwasa, T. Yoshizawa, and S. I. Ohnishi. 1981. Flash induced fast change in surface potential and fluidity of purple membrane studied by spin label method. *Photochem. Photobiol.* 33:467–474.
11. Ahl, P., and R. Cone. 1982. Photocycling and noncycling bacteriorhodopsin chromophores undergo different rational displacements within the purple membrane. *Biophys. J.* 37(2, Pt. 2):229*a*. (Abstr.)
12. Korenstein, A., and B. Hess. 1977*a*. Hydration effects on the photocycle of bacteriophodopsin in the layers of purple membrane. *Nature. (Lond.)*. 270:184–186.
13. Korenstein, R., and B. Hess. 1977*b*. Hydration effects on cis-trans isomerization of bacteriorhodopsin. *FEBS (Fed. Eur. Biochem. Soc.) Lett.* 82:7–11.
14. Hwang, S. B., J. I. Korenbrot, and W. Stoeckenius. 1978. Transient photovoltages in purple membrane multilayers. Charge displacement in bacteriorhodopsin and its photo intermediates. *Biochem. Biophys. Acta*. 509:300–317.
15. Rothchild, K. J., R. Sanches, and N. A. Clark. 1982. Infrared

absorption of photoreceptor and purple membrane. *Methods Enzymol.* 88:696–714.

16. Bagley, K., G. Dollinger, L. Eisenstein, A. K. Singh, and L. Zimanyi. 1982. Fourier transform infrared difference spectroscopy of bacteriorhodopsin and its photoproducts. *Proc. Natl. Acad. Sci. USA.* 79:4972–4976.
17. Seka, W., J. Soures, O. Lewis, J. Bunkenburg, D. Brown, S. Jacobs, G. Mourou, and J. Zimmerman. 1980. High-power phosphate-glass laser systems design and performance characteristics. *Appl. Optics.* 19:409–419.
18. Yaakobi, B., P. Bourke, Y. Contuire, J. Delettrez, J. M. Forsyth, R. D. Frankel, L. M. Goldman, R. L. McCrory, W. Seka, and J. M. Soures. 1981. High x-ray conversion efficiency with target irradiation by a frequency tripled Nd:glass laser. *Optic Comm.* 38:196–200.
19. Seka, W., S. D. Jacobs, J. E. Rizzo, R. Boni, and R. S. Craxton. 1980. Demonstration of high efficiency third harmonic conversion of high power Nd:glass laser radiation. *Optic Comm.* 34:469–473.
20. Henke, B. L., and J. W. M. DuMond. 1955. Submicron structure determination by long wavelength x-ray diffraction. *J. Appl. Phys.* 26:903–917.
21. Elliott, A. 1966. The use of toroidal reflecting surfaces in x-ray diffraction cameras. *J. Sci. Instrum.* 42:312–316.
22. Reynolds, G. T., J. R. Milch, and S. M. Gruner. 1977. Image intensification of x-ray diffraction patterns from biological structures. *IEEE. (Inst. Electr. Electron. Eng.) Trans. Nucl Sci.* NS-24:501–510.
23. H. Staerk, R. Mitzkus, and H. Meyer. 1981. Performance of SIT vidicons when exposed to transient light signals. *Appl. Optics.* 20:471–476.
24. G. W. Liesegang, and P. D. Smith. 1981. Improving vidicon linearity in the pulsed illumination mode. *Appl. Optics* 20:2604–2605.
25. C. R. Goldschmidt, O. Kalisky, T. Rosenfeld, T. M. Ottolenghi. 1977. The quantum efficiency of the bacteriorhodopsin photocycle. *Biophys. J.* 17:179–184.
26. O. Kalisky, C. R. Goldschmidt, and M. Ottolenghi. 1977. On the photocycle and light adaptation of dark-adapted bacteriorhodopsin. *Biophys. J.* 19:185–189.
27. Henderson, R. J. 1975. The structure of the purple membrane from halobacterium halobium: analysis of the x-ray diffraction pattern. *Mol. Biol.* 93:123–138.
28. Blaurock, A. E. 1975. Bacteriorhodopsin: a trans-membrane pump containing α-helix. *J. Mol. Biol.* 93:139–158.
29. Kataoka, M., and T. Ueki. 1980. The significance of the radial autocorrelation function for the interpretation of equatorial diffraction from biological membranes. *Acta Crystallogr. Sect. A Cryst. Phys. Diffr. Theor. Gen. Crystallogr.* A36:282–287.
30. Zaccai, G., and D. J. Gilmore. 1979. Areas of hydration in the purple membrane of *Halobacterium halobium:* a neutron diffraction study. *J. Mol. Biol.* 132:181–191.
31. Stamatoff, J., R. H. Lozier, and S. Gruner. 1982. X-ray diffraction studies of light interactions with bacteriorhodopsin. *Methods Enzymol.* 88:282–286.
32. Nagle, J. F., and H. J. Morowitz. 1978. Molecular mechanisms for proton transport in membranes. *Proc. Natl. Acad. Sci. USA.* 75:298–302.
33. Lewis, A., J. Spoonhower, R. A. Bogomolni, R. Lozier, and W. Stoeckenius. 1974. Tunable laser resonance Raman spectroscopy of bacteriorhodopsin. *Proc. Natl. Acad. Sci. USA.* 71:4462–4466.
34. Becher, B., and J. Cassim. 1977. Effects of bleaching and regeneration on the purple membrane structure of *Halobacterium Halobium. Biophys. J.* 19:285–297.
35. Bogomolni, R. A., L. Stubbs, and J. K. Lanyi. 1978. Illumination-dependent changes in the instrinsic fluorescence of bacteriorhodopsin. *Biochemistry.* 17:1037–1041.
36. Becher, B., F. Tokunaga, and Th. G. Ebrey. 1978. Ultraviolet and visible absorption spectra of the purple membrane protein and the photocycle intermediates. *Biochemistry.* 17:2293–2300.
37. Hess, B., and D. Kuschmitz. 1979. Kinetic interaction between aromatic residues and the retinal chromophore of bacteriorhodopsin during the photocycle. *FEBS (Fed. Eur. Biochem. Soc.) Lett.* 100:334–340.
38. D. Beece, S. F. Bowne, J. Czege, L. Eisentein, H. Frauenfelder, D. Good, M. C. Marden, J. Marque, P. Ormos, L. Reinisch, and K. T. Yue. 1981. The effect of viscosity on the photocycle of bacteriorhodopsin. *Photochem. Photobiol.* 33:517–522.
39. J. A. Abate, L. Lund, D. Brown, S. Jacobs, S. Refermat, J. Kelly, M. Gavin, S. Walobillig, and O. Lewis. 1981. Active mirror: a large-aperture medium-repetition rate Nd:glass amplifier. *Appl. Optics.* 20:351–362.